PERGAMON

Continental Shelf Research 22 (2002) 1857–1866

CONTINENTAL SHELF RESEARCH

www.elsevier.com/locate/csr

Variability of suspended-sediment concentration at tidal to annual time scales in San Francisco Bay, USA

David H. Schoellhamer*

U.S. Geological Survey, Placer Hall, 6000 J Street, Sacramento, CA 95819, USA

Received 10 November 2000; accepted 3 December 2001

Abstract

Singular spectrum analysis for time series with missing data (SSAM) was used to reconstruct components of a 6-yr time series of suspended-sediment concentration (SSC) from San Francisco Bay. Data were collected every 15 min and the time series contained missing values that primarily were due to sensor fouling. SSAM was applied in a sequential manner to calculate reconstructed components with time scales of variability that ranged from tidal to annual. Physical processes that controlled SSC and their contribution to the total variance of SSC were (1) diurnal, semidiurnal, and other higher frequency tidal constituents (24%), (2) semimonthly tidal cycles (21%), (3) monthly tidal cycles (19%), (4) semiannual tidal cycles (12%), and (5) annual pulses of sediment caused by freshwater inflow, deposition, and subsequent wind-wave resuspension (13%). Of the total variance 89% was explained and subtidal variability (65%) was greater than tidal variability (24%). Processes at subtidal time scales accounted for more variance of SSC than processes at tidal time scales because sediment accumulated in the water column and the supply of easily erodible bed sediment increased during periods of increased subtidal energy. This large range of time scales that each contained significant variability of SSC and associated contaminants can confound design of sampling programs and interpretation of resulting data. Published by Elsevier Science Ltd.

Keywords: Estuarine sedimentation; River discharge; Singular spectrum analysis; Suspended sediment; Tides; Wind waves

1. Introduction

Various processes cause suspended-sediment concentration (SSC) in an estuary to vary over time scales ranging from seconds to years. Turbulence, semidiurnal tides, diurnal tides, other tidal harmonics, lower frequency tidal cycles, wind waves, watershed inflow, and climatic variability cause SSC to vary with time. Lower frequency variability is more difficult to quantify because continuous SSC time series are difficult to collect for a long duration (months) and analytical tools typically require complete series with no missing data.

Consideration of subtidal variability of SSC is necessary for evaluating some water quality objectives for San Francisco Bay. Mercury is one of many contaminants associated with sediment particles, so SSC is a good estimator of mercury concentration (Schoellhamer, 1997). The water-quality objective for mercury in the water column is based on a 4-day average concentration. The 4-day averaging period virtually eliminates the influence of semidiurnal and diurnal tides, leaving subtidal processes to determine whether the

*Tel.: +1-916-278-3126; fax: +1-916-278-3071.
E-mail address: dschoell@usgs.gov (D.H. Schoellhamer).

0278-4343/02/$ - see front matter Published by Elsevier Science Ltd.
PII: S0278-4343(02)00042-0

water-quality objective is satisfied. Schoellhamer (1997) found that the objective often is violated during spring tides and is satisfied during neap tides because tidal energy, SSC, and mercury concentration covary.

In this study, 6 yr of SSC data collected in San Francisco Bay were analyzed to determine the relative importance of various time scales and associated processes. Calibrated optical backscatterance sensors made measurements every 15 min, but some data were invalidated by biological fouling. A modified version of singular spectral analysis that accounts for missing data was used to determine the components of the SSC time series.

2. Methods

2.1. SSC data

The U.S. Geological Survey has established a network of eight sites in San Francisco Bay at which SSC is monitored (Buchanan and Ruhl, 2000). Optical backscatterance sensors are deployed at two depths at each site and measurements are collected automatically every 15 min. Water samples are collected periodically, analyzed for SSC, and the results of these analyses are used to calibrate the sensors. An SSC time series collected at middepth (4 m above the bed) at Point San Pablo (Fig. 1) was chosen for analysis because it is one of the longer (almost 6 yr) and more complete (73.5% valid) time series available (Fig. 2). Water-level data also are collected at Point San Pablo every 15 min (Buchanan, 1999). Most freshwater inflow enters San Francisco Bay at Chipps Island and is estimated by the Interagency Ecological Program (2001). Wind-speed data were available at Carneros in the southern Napa Valley across San Pablo Bay from Point San Pablo (California Irrigation and Management Information System, 1999).

2.2. SSAM data

SSA is essentially a principal components analysis (PCA) in the time domain that extracts information from short and noisy time series without prior knowledge of the dynamics affecting the time series (Vautard et al., 1992; Dettinger et al., 1995). The objective of PCA is to take a set of (often) time-dependent variables and find a new set of variables that are uncorrelated and, thus, measure different dimensions of the data with most of the variance contained in fewer variables (Manly, 1992). Principal components are calculated by multiplying the eigenvectors of the covariance matrix and the data. The variance of each principal component is equal to its eigenvalue and the sum of the variances of the principal components is equal to the sum of the variances of the original variables. Each principal component describes a known fraction of the variance of the original variables. Principal components are sorted by decreasing variance and, typically, the first several contain most of the variance.

SSA is similar to PCA in that M variables are created by lagging the time series of interest from zero to $M-1$ time steps (Vautard et al., 1992). Eigenvectors and eigenvalues of the lagged autocorrelation matrix and principal components are calculated. The time series is decomposed into reconstructed components (RCs) by multiplying the principal components and eigenvectors. With the sorting used, the RCs are ordered by decreasing information about the original time series. Most of the variance is contained in the first several RCs, which typically are nearly periodic with one or two dominant periods, and most or all of the remaining RCs contain noise. A pair of RCs containing similar variance normally represents each period that is smaller than M with significant energy in the original time series. SSA typically is successful at identifying periods in the range $0.2M$—M. One or two RCs contain variations in the time series with periodicities greater than M. SSA has been applied to continuous blocks of SSC data from San Francisco Bay that were 14–70 days long; several tidal signals were identified and the fortnightly spring/neap tidal cycle accounted for about one-half of the variance of SSC (Schoellhamer, 1996).

SSA was modified to permit missing data (SSAM) and the reader should refer to Schoellhamer (2001b) for details. This modification eliminates the need to screen, fill, and subdivide time

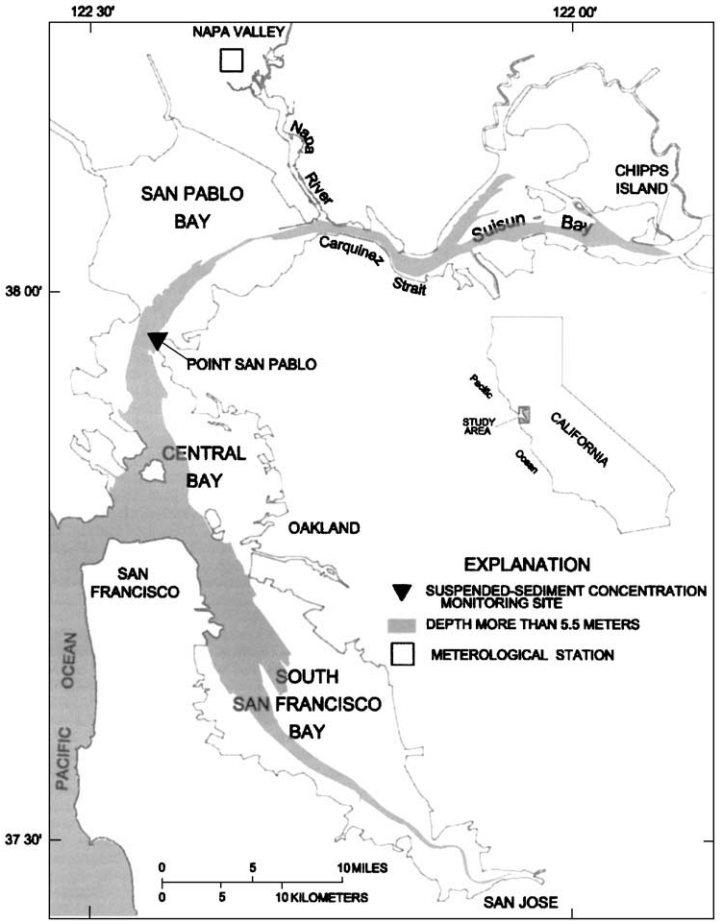

Fig. 1. Study area.

series prior to applying SSA and allows analysis of longer, but incomplete, time series. Missing values are ignored when computing the lagged autocorrelation matrix. When computing each value in a principal component series, if the fraction of missing data within window $M<f$, then that value is assigned a missing value. In this study, f was set equal to 0.5. If any principal component value is missing, then the corresponding RC value also will be missing.

Schoellhamer (2001b) successfully tested SSAM with corrupted synthetic SSC time series. Noise, long data gaps, and randomly assigned missing values were used to corrupt a synthetic time series. Despite these defects, SSAM was able to reconstruct the known synthetic components of the time series.

2.3. Application of SSAM

SSAM was applied to the SSC time series from Point San Pablo and to decimated time series, which allowed for a constant window size $M=120$. Window size M limits the periods that can be recognized by SSAM, and as M increases, the computational requirements increase. Initially, SSAM was applied to the 15-min data with a 30-h window (pass 1, Table 1). Then the data were decimated with a centred, 1.25-h running mean (averaging five time steps). If more than one-half

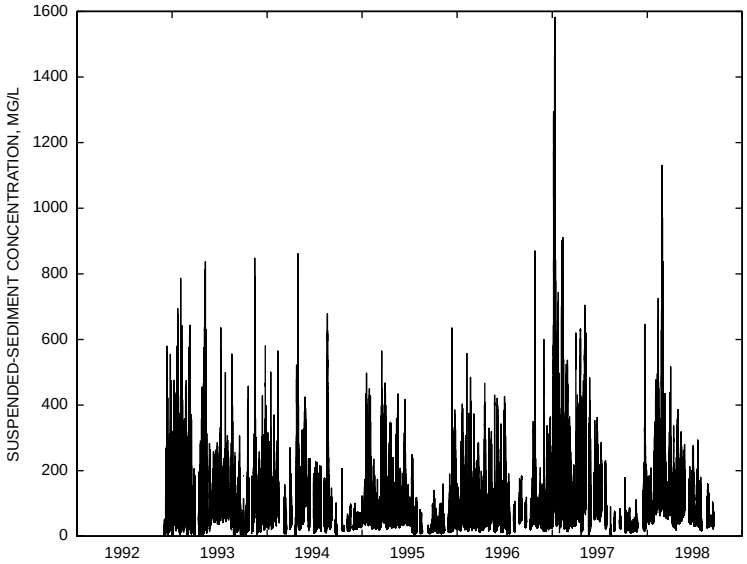

Fig. 2. SSC at middepth at Point San Pablo.

Table 1
SSAM passes to SSC data

Pass	Data time step (hours)	SSAM window size (hours)	Optimal range of periods for SSAM (hours)
1	0.25	30	6–30
2	1.25	150	30–150
3	6.25	750	150–750
4	31.25	3750	750–3750
5	156.25	18,750	3750–18,750

SSAM, singular spectrum analysis for time series with missing data.

(three or more) of the values were valid, the corresponding mean was calculated, otherwise the corresponding mean was assigned a missing value. SSAM was applied to the decimated data (1.25-h time step) with a window size of 120 (150 h, pass 2, Table 1). The decimation and SSAM windows were increased sequentially by factors of five for passes 3–5 to allow all periods from 0.25 to 781.25 days to fall within the optimal range of analysis for one application of SSAM (Table 1). Each SSAM pass to the data removed high frequency ($M < 120$) variability from the signal, reducing the variance of the remaining time series. To calculate the relative contribution of an RC from passes 2–5 to the original time series, the eigenvalue was multiplied by the ratio of the variance of the time series used for that pass to the variance of the original time series.

3. Results

Several time scales of variability were identified by the analysis and 89% of the total variability was attributable to five specific physical processes (Fig. 3). The five time scales of variability that were identified are described below: (1) diurnal, semidiurnal, and other higher frequency tidal constituents (24%), (2) semimonthly tidal cycles (21%), (3) monthly tidal cycles (19%), (4) semi-annual tidal cycles (12%), and (5) annual pulses of sediment caused by freshwater inflow, deposition, and subsequent wind-wave resuspension (13%). Pass 5 produced an interannual RC (not shown) that contained 3% of the variance. This RC was not obviously related to climatic variations but was, in part, attributable to two shifts in sensor calibration after severe fouling and a change in the calibration method.

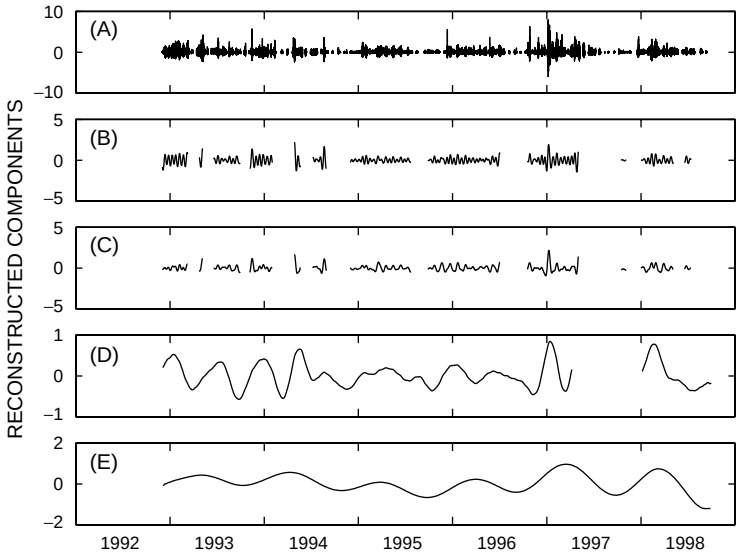

Fig. 3. RC primarily containing variability due to (A) diurnal, semidiurnal, and other higher frequency tidal constituents (24% of total SSC variance, from pass 1), (B) semimonthly tidal cycles (21%, pass 3), (C) monthly tidal cycles (19%, pass 3), (D) semiannual tidal cycles (12%, pass 4), and (E) annual pulses of sediment caused by freshwater inflow, deposition, and subsequent wind-wave resuspension (13%, pass 5).

3.1. Diurnal, semidiurnal, and other higher frequency tidal constituents

The first pass of SSAM with a window size of 30 h separated the tidal constituents (Fig. 3A) from the subtidal components. Tidal constituents account for 24% of the total variability and contain semidiurnal, diurnal, terdiurnal, and quarter diurnal constituents. An example of 3 days of tidal variability and the corresponding SSC RC is shown in Fig. 4. During this time, three major SSC maxima occurred per day. This probably occurred because of advection of turbid water from San Pablo Bay, and perhaps resuspension, increased SSC during both ebb tides, sediment resuspended during the stronger flood tide, and SSC did not increase during the weaker flood tide.

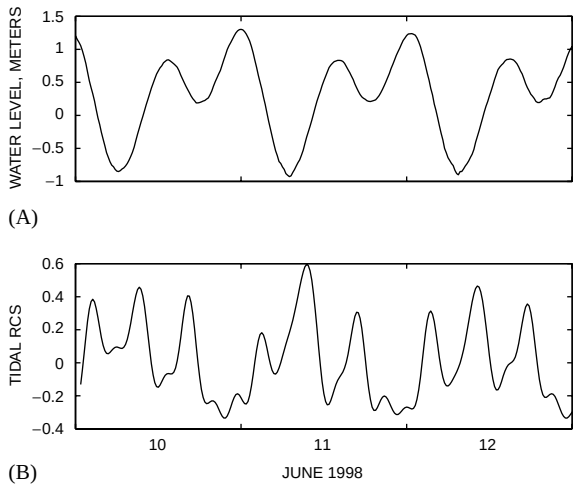

Fig. 4. Water level at Point San Pablo (A) and reconstructed components primarily containing tidal variability due to diurnal, semidiurnal, and other higher frequency tidal constituents (B), June 10–12, 1998.

3.2. Semimonthly tidal cycles

When the principal semidiurnal tidal constituents ($M2$ and $S2$) are in phase every 14.76 days spring tides result and when the principal diurnal constituents ($O1$ and $K1$) are in phase every 13.66 days, tropic tides result. These semimonthly perturbations of tidal range alter the tidal energy and SSC (Fig. 5). For example, greater SSC during spring tides could be caused by greater resuspension of bottom sediment by greater tidal currents

or by increased tidal excursion that is large enough to transport turbid water from shallower water to Point San Pablo during ebb tides (Ruhl et al., 2001). Tides predominantly are semidiurnal, so spring tides have a greater effect on SSC than tropic tides. SSAM was not able to differentiate between the effects of spring and tropic tides on SSC.

3.3. Monthly tidal cycles

Other tidal constituents combine to vary tidal energy on a monthly time scale, with a resulting response in SSC (Fig. 6). Spring and tropic tides combine to create strong spring tides (solstitial tides) during the summer and winter solstices and combine to create the weakest (equinoctial) tides during the spring and autumn equinoxes. Variability of the monthly RC is greatest during solstices and smallest during equinoxes.

3.4. Semiannual tidal cycles

Solstitial and equinoctial tides also create a semiannual SSC signal (Fig. 7). The semiannual variation results in SSC that is greater during solstices than during equinoxes.

3.5. Annual influx, deposition, and resuspension of sediment

In San Francisco Bay, an annual cycle of deposition and resuspension begins with large influx of sediment during large freshwater flows in winter (Goodwin and Denton, 1991; Schoellhamer, 1997; Oltmann et al., 1999). The first freshwater pulse in winter delivers a relatively large amount of sediment compared to subsequent pulses. Much of this new sediment deposits in shallow water subembayments. Stronger westerly winds during spring and summer cause wind-wave resuspension of bottom sediment in these shallow waters and increase SSC (Ruhl et al., 2001). The ability of wind to increase SSC is greatest early in the spring, when unconsolidated fine sediments easily can be resuspended. As the fine sediments are winnowed from the bed, however, the remaining sediments become progressively less erodible (Conomos and Peterson, 1977; Krone, 1979; Nichols and Thompson, 1985). The annual variability of SSC detected by SSAM reflects this

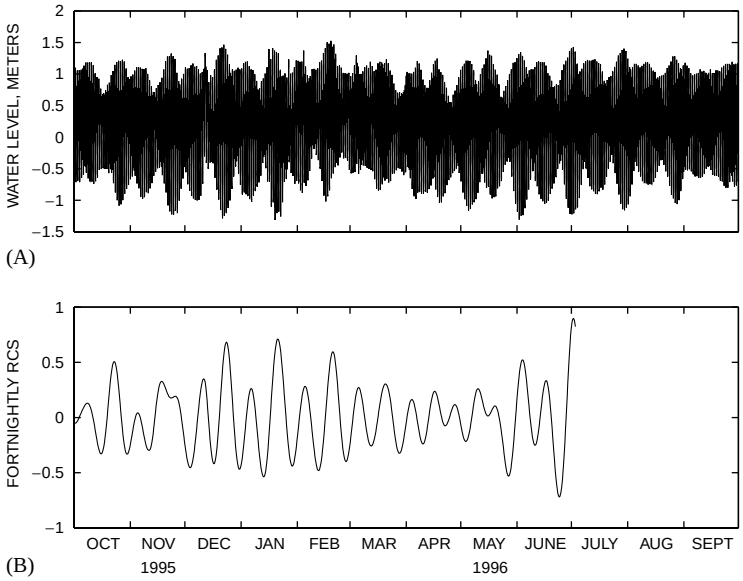

Fig. 5. Water level at Point San Pablo (A) and reconstructed components primarily containing variability associated with semimonthly tidal cycles, water year 1996 (B).

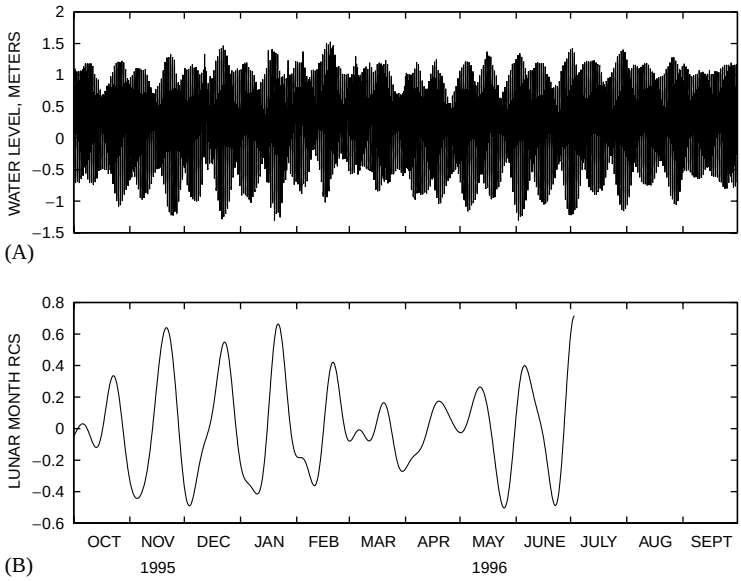

Fig. 6. Water level at Point San Pablo (A) and reconstructed components primarily containing variability associated monthly tidal cycles, water year 1996 (B).

annual cycle of sediment influx, deposition, and resuspension (Fig. 8).

4. Discussion

SSC variability caused by diurnal and semidiurnal tides is most obvious in an estuary but accounts for only 24% of the SSC variance observed in this study. Recognizable variability at longer (subtidal) time scales accounted for 65% of the variance of SSC and noise accounted for the remaining variance (11%).

Processes at subtidal time scales accounted for more variance of SSC than processes at tidal time scales because sediment accumulated in the water column and the supply of easily erodible bed sediment increased during periods of increased subtidal energy. Sediment tended to accumulate in the water column during periods of stronger tides or wind because the duration of slack water was on the order of minutes in San Francisco Bay and, thus, limited deposition. For example, suspended sediment accumulates in the water column as a spring tide is approached and slowly deposits as a neap tide is approached (Schoellhamer, 1996). During a tidal cycle, the exchange of sediment between the water column and bed via deposition and resuspension, the supply of easily erodible bed sediment, and SSC increase as the subtidal energy increases (Schoellhamer et al., 2000). In addition, the supply of erodible sediment that experiences wind-wave resuspension in shallow water varies seasonally (Conomos and Peterson, 1977; Krone, 1979; Nichols and Thompson, 1985).

Shorter, continuous SSC time series from other estuaries also indicate that SSC varies with semimonthly and monthly tidal cycles. Semimonthly spring/neap tidal cycle variability of SSC has been observed in many estuaries where continuous SSC time series of 8 days to 13 months in duration have been collected (Uncles et al., 1994; Wolanski et al., 1995; Kappenberg et al., 1996; Lindsay et al., 1996; Fettweis et al., 1998). To quantify the contributions of various tidal periods to SSC in the Seine estuary, Guezennec et al. (1999) applied spectral analysis to 5 months of SSC data. Power spectral density was significant at 4 periods. Energy at semimonthly and semidiurnal periods was equal. Energy at monthly and

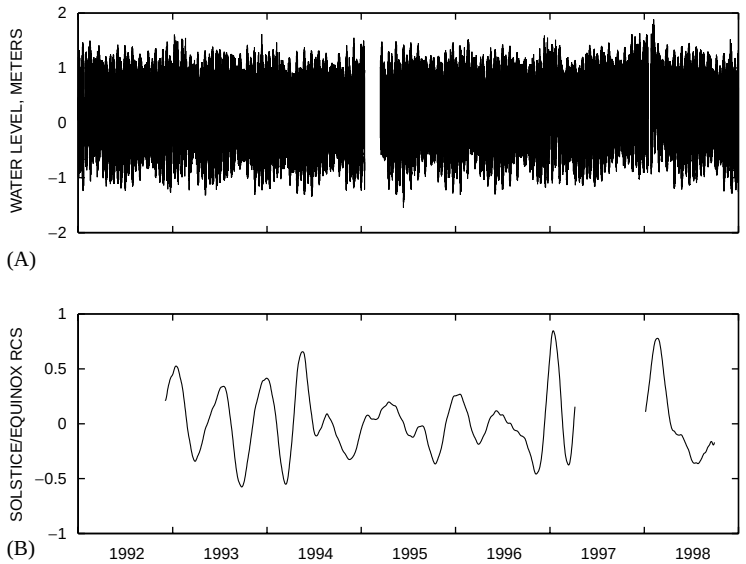

Fig. 7. Water level at Point San Pablo (A) and reconstructed components primarily containing variability associated with semiannual tidal cycles (B).

quarter diurnal periods was equal and contained almost one-half of the energy contained in the first two periods. The ratio of semimonthly and monthly variability to tidal cycle variability was about one in the Seine estuary compared with 1.7 in San Francisco Bay. SSC varied semiannually in San Francisco Bay, but this was not observed by these studies, possibly because the time series were shorter or semiannual variability was unimportant or masked by other processes.

The annual cycle of SSC and freshwater flow in San Francisco Bay differs from that observed in Weser and Elbe estuaries where multiyear SSC measurements also have been made. In San Francisco Bay, SSC is greatest in spring when wind waves resuspend sediment delivered during high winter flows (Fig. 8). In the Weser and Elbe estuaries, however, high-freshwater flows destroy the estuarine turbidity maxima (ETM) and reduce SSC (Grabemann et al., 1996). In San Francisco Bay during low flows in summer and autumn, SSC decreases as the supply of erodible sediment decreases. In the Weser and Elbe estuaries during low flow, SSC increases as sediment accumulates in the ETM. Point San Pablo is not in an ETM but the same annual cycle that includes decreasing SSC during low flow is observed in San Francisco Bay in Carquinez Strait (Buchanan and Ruhl, 2000; Fig 8) where there is an ETM (Jay and Musiak, 1994; Schoellhamer, 2001a).

The large range of time scales present in the SSC time series from San Francisco Bay pose great technical challenges for monitoring and management of the Bay. Semiannual and annual variability are more difficult to quantify because time series of long duration (years) are difficult to collect and analyze. Variability at these larger time scales is significant (25%) in San Francisco Bay and can confound analysis of SSC and related data, such as sediment-associated contaminants, if the sampling design is short in duration or coarse, relative to the larger time scales. Tidal variability also is significant, however, and can mask subtidal variability if a sampling program is short in duration, relative to the subtidal time scales, and coarse, relative to tidal time scales. Sampling programs for SSC and related data should consider variability at all significant time scales to reduce the potential of an interpretive error.

This analysis identified five time scales of variability and associated processes, but annual riverine influx of sediment was not identified as a

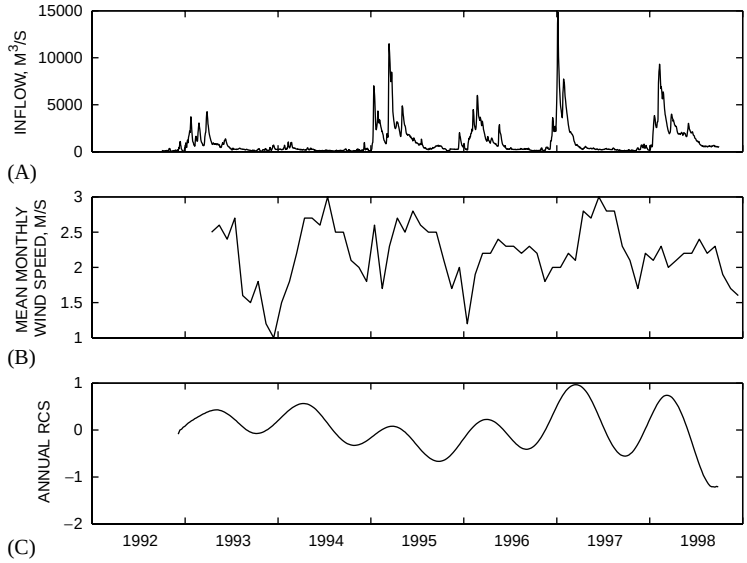

Fig. 8. Inflow at Chipps Island (A), mean monthly wind speed at Carneros (B), and reconstructed components primarily containing annual variability (C).

distinct process. Riverine influx of sediment to San Francisco Bay is greatest during the winter rainy season. This new sediment deposits on the bottom of the Bay, where it begins a cycle of resuspension, transport, and deposition. Thus, the suspended mass in the Bay is almost exclusively derived from resuspension by currents and wind waves, not riverine input. The RCs primarily contain resuspension signals, not influx signals.

5. Conclusions

Singular spectrum analysis for time series with missing data was used to reconstruct components of a 6-yr time series of suspended sediment concentration from San Francisco Bay. The time scales of variability ranged from tidal to annual. Physical processes that controlled SSC and their contribution to the total variance of SSC were (1) diurnal, semidiurnal, and other higher frequency tidal constituents (24%), (2) semimonthly tidal cycles (21%), (3) monthly tidal cycles (19%), (4) semiannual tidal cycles (12%), and (5) annual pulses of sediment caused by freshwater inflow, deposition, and subsequent wind-wave resuspension (13%). 89% of the total variance was explained and subtidal variability (65%) was greater than tidal variability (24%). This large range of time scales with significant variability of SSC and associated contaminants can confound design of sampling programs and interpretation of resulting data. Processes at subtidal time scales accounted for more variance of SSC than processes at tidal time scales because sediment accumulated in the water column and the supply of easily erodible bed sediment increased during periods of increased subtidal energy.

Acknowledgements

I thank Paul Buchanan, Rob Sheipline, Brad Sullivan, and Rick Adorador for collecting the SSC data and Mike Dettinger, Cathy Ruhl, and Carol Sanchez for their assistance. The San Francisco District of the U.S. Army Corps of Engineers, as part of the Regional Monitoring Program for Trace Substances, supported SSC data collection at Point San Pablo.

References

Buchanan, P.A., 1999. Specific conductance, water temperature, and water level data, San Francisco Bay, California, water year 1998. Interagency Ecological Program Newsletter 12 (4), 46–51.

Buchanan, P.A., Ruhl, C.A., 2000. Summary of suspended-solids concentration data, San Francisco Bay, California, water year 1998. U.S. Geological Survey Open-File Report 00-88, p. 41.

California Irrigation and Management Information System, 1999. URL: http://wwwdla.water.ca.gov/cgi-bin/cimis/cimis/hq/main.pl.

Conomos, T.J., Peterson, D.H., 1977. Suspended-particle Transport and Circulation in San Francisco Bay, an Overview. Academic Press, New York. Estuarine Processes 2, 82–97.

Dettinger, M.D., Ghil, M., Strong, C.M., Weibel, W., Yiou, P., 1995. Software expedites singular-spectrum analysis of noisy time series. EOS 76(2), 12, 14 and 21.

Fettweis, M., Sas, M., Monbaliu, J., 1998. Seasonal, neap-spring and tidal variation of cohesive sediment concentration in the Scheldt Estuary, Belgium. Estuarine, Coastal and Shelf Science 47, 21–36.

Goodwin, P., Denton, R.A., 1991. Seasonal influences on the sediment transport characteristics of the Sacramento River. Proceedings of the Institute of Civil Engineers, Part 2, 91, 163–172.

Grabemann, I., Kappenberg, J., Krause, G., 1996. Comparison of the dynamics of the turbidity maxima in two coastal plain estuaries. Archiv fuer Hydrobiogie Special Issues and Advance Limonology 47, 195–205.

Guezennec, L., Lafite, R., Dupont, J.-P., Meyer, R., Boust, D., 1999. Hydrodynamics of suspended particulate matter in the tidal freshwater zone of a macrotidal estuary (the Seine Estuary, France). Estuaries 22 (3A), 717–727.

Interagency Ecological Program, 2001. Dayflow program documentation and data. URL: http://www.iep.ca.gov/dayflow/index.html.

Jay, D.A., Musiak, J.D., 1994. Particle trapping in estuarine tidal flows. Journal of Geophysical Research 99 (C10), 20445–20461.

Kappenberg, J., Schymura, G., Kuhn, H., Fanger, H.U., 1996. Spring-neap variations of suspended sediment concentration and transport in the turbidity maximum of the Elbe estuary. Archiv fuer Hydrobiogie Special Issues and Advance Limonology 47, 323–332.

Krone, R.B., 1979. Sedimentation in the San Francisco Bay system. In: Conomos, T.J. (Ed.), San Francisco Bay, the Urbanized Estuary. Pacific Division of the American Association for the Advancement of Science, San Francisco, pp. 347–385.

Lindsay, P., Balls, P.W., West, J.R., 1996. Influence of tidal range and river discharge on suspended particulate matter fluxes in the Forth estuary (Scotland). Estuarine, Coastal and Shelf Science 42, 63–82.

Manly, B.F.J., 1992. Multivariate Statistical Methods, a Primer. Chapman & Hall, New York.

Nichols, F.H., Thompson, J.K., 1985. Time scales of change in the San Francisco Bay benthos. Hydrobiologia 192, 121–138.

Oltmann, R.N., Schoellhamer, D.H., Dinehart, R.L., 1999. Sediment inflow to the Sacramento-San Joaquin Delta and the San Francisco Bay. Interagency Ecological Program Newsletter 12 (1), 30–33.

Ruhl, C.A., Schoellhamer, D.H., Stumpf, R.P., Lindsay, C.L., 2001. Use of remote sensing images of San Francisco Bay to analyze suspended-sediment concentrations. Estuarine, Coastal and Shelf Science 53, 801–812.

Schoellhamer, D.H., 1996. Factors affecting suspended-solids concentrations in South San Francisco Bay, California. Journal of Geophysical Research 101 (C5), 12087–12095.

Schoellhamer, D.H., 1997. Time series of SSC, salinity, temperature, and total mercury concentration in San Francisco Bay during water year 1996. 1996 Annual Report of the Regional Monitoring Program for Trace Substances, pp. 65–77.

Schoellhamer, D.H., 2001a. Influence of salinity, bottom topography, and tides on locations of estuarine turbidity maxima in northern San Francisco Bay. In: McAnally, W.H., Mehta, A.J. (Eds.), Coastal and Estuarine Fine Sediment Transport Processes. Elsevier Science B.V., Amsterdam, pp. 343–357. URL: http://ca.water.usgs.gov/abstract/sfbay/elsevier0102.pdf.

Schoellhamer, D.H., 2001b. Singular spectrum analysis for time series with missing data. Geophysical Research Letters, 28(16), 3187–3190. URL: http://ca.water.usgs.gov/ja/grl/ssam.pdf.

Schoellhamer, D.H., Burau, J.R., Brennan, M.L., Monismith, S.G., 2000. Transfer of cohesive sediment between the bed and water column at a site in San Francisco Bay, USA. Proceedings of the Sixth International Conference on Nearshore and Estuarine Cohesive Sediment Transport Processes, Delft, The Netherlands, September 4–8, 2000, pp. 8–9.

Uncles, R.J., Barton, M.L., Stephens, J.A., 1994. Seasonal variability of fine-sediment concentrations in the turbidity maximum region of the Tamar Estuary. Estuarine, Coastal and Shelf Science 38, 19–39.

Vautard, R., Yiou, P., Ghil, M., 1992. Singular-spectrum analysis: a toolkit for short, noisy, chaotic signals. Physica D 58, 95–126.

Wolanski, E., King, B., Galloway, D., 1995. Dynamics of the turbidity maximum in the Fly River estuary, Papua New Guinea. Estuarine, Coastal and Shelf Science 40, 321–337.